Journal of Materials Chemistry C

Accepted Manuscript

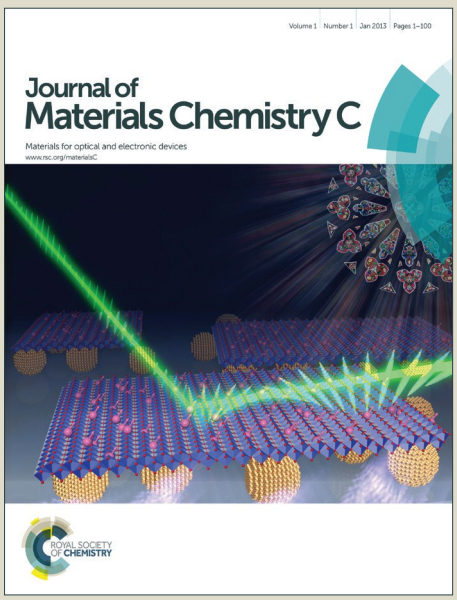

ROYAL SOCIETY OF CHEMISTRY

www.rsc.org/materialsC

Journal Name

ARTICLE

Electrochromic properties of vertically aligned Ni-doped WO_3 nanostructure films and their application in complementary electrochromic devices

Received 00th January 20xx,
Accepted 00th January 20xx

DOI: 10.1039/x0xx00000x

www.rsc.org/

Junling Zhou, Youxiu Wei, Gui Luo, Jianming Zheng, Chunye Xu*

Tungsten trioxide (WO_3) is a promising electrochromic material for potential applications in architectural and automotive smart windows. Nanostructured WO_3 have attracted particular attention in the past few years due to their potential advantages in electrochromic properties. Here, Ni-doped WO_3 nanostructured films were achieved by seed-free hydrothermal method directly on transparent conducting substrates. The influences of Ni doping on nanostructure and electrochromic properties of WO_3 films are investigated. Compared to pure WO_3 films, Ni doping can increase crystal defects and induce to significant changes of nanostructure, thus affecting the electrochromic performance of WO_3 films. Low concentration Ni-WO_3 films achieved vertically aligned nanorods morphology, ultrahigh optical modulation (over 85% from 600 to 900 nm), high coloration efficiency (60.5 mc^2 C^{-1} at 600 nm) and excellent cycling stability for about 5500 cycles. Finally, the complementary electrochromic device assembled with 1.5% Ni-WO_3 and NiO-based films exhibited vivid color change from transparent to black (x= 0.326, y=0.369, Y_L%= 3.29%) with maximum transmittance of about 3.5% at dark state.

1 Introduction

Electrochomic device (ECD) attracts extensive attention for its potential applications in various fields, such as smart windows, electronic displays, electrochromic mirrors and so on.[1-5] ECD is a kind of smart device which is able to reversibly change its optical properties such as transmittance, absorption and reflection by external electric stimulation. A typical ECD consists of five functional layers, including two different electrocheomic layers separated by an ion conductor layer, and two transparent conducting layer. Electrochomic materials are the active component in an ECD, which dominate the color changing performance. They can be generally classified into two groups, anodic (coloring under ion extraction) and cathodic (coloring under ion insertion) electrochromic materials. Anodic electrochromic film (for example NiO , IrO_2 and polyaniline) and cathodic film (for example WO_3 , MoO_3 and polythiophene derivative) can be incorporated into a complementary ECD, in which both of the films could be colored (or bleached) under a certain potential. [6-15]

Among various electrochromic materials, amorphous WO_3 has been extensively investigated, because of its excellent optical modulation and stability. Unfortunately, the crystalline WO_3 film, comparing to amorphous WO_3, exhibits low optical modulation and coloration efficiency, limiting its further commercialization.[16] It is widely recognized that nanostructured crystalline WO_3 films, compared with bulk-structure ones, can achieve larger optical contrast ratio, faster switching speed and higher coloration efficiency by providing much more effective contact area with electrolyte and increasing the diffusion rate of ions.[17-19] Recently, one dimensional (1D) WO_3 nanostructures synthesized by hydrothermal method have attracted intense interest for superior charge transport properties and facile processing.[19-22] Cai and Zhang et al synthesized vertically aligned hierarchical WO_3 nano-achitecture arrays directly on FTO-coated glass by preparing crystalline WO_3 seeds layer on the glass, showing enhanced electrochromic properties.[19, 20] Moreover, the coloration efficiency of crystalline WO_3 films could be further improved by metal ions doping, such as Ti and Ni.[23-26] Green et al prepared Ni-WO_3 films by DC co-sputtering method and found that low concentration of Ni doping could enhanced optical modulation of WO_3 films.[24, 25] Lately, Cai et al combined Ti doping with WO_3 nanostructure, and synthesized star-like Ti-doped WO_3 nanostructure film by hydrothermal processing.[23] The Ti-WO_3 nanostructure films demonstrated low charge transfer resistance, high color efficiency, and fast switching speed, but the optical modulation (49.1% at 750 nm) is still insufficient compared with typical amorphous ones (67.6% at 632 nm).[16, 23] Here, we attempted to further improve optical

*Hefei National Laboratory for Physical Sciences at the Microscale, CAS Key Laboratory of Soft Matter Chemistry, Department of Polymer Science and Engineering, University of Science and Technology of China, Hefei 230026, PR China. *E-mail: chunye@ustc.edu.cn; Tel &Fax: +86-551-6360-3459*

† Electronic Supplementary Information (ESI) available: XPS survey data and fitting peaks of W 4f XPS spectra. SEM images of 0-3% Ni-WO_3 films and cross section of 0.5% and 1.5% Ni-WO_3 films. TEM images with larger magnification of 2.5% Ni-WO_3 sample. Equivalent circuit used for fitting EIS data and corresponding fitting parameters. Transmittance spectra of Li-Ti-NiO films and CIE color space of liquid ECD in bleached and colored state. Video of liquid and solid ECD.See DOI: 10.1039/x0xx00000x

modulation of crystal WO_3-based films by Ni doping and nanostructure modification through simple hydrothermal method.

In our present study, we synthesized nanostructured Ni-doped WO_3 films directly on ITO glass by seed-free hydrothermal method, and investigated the electrochromic properties of these films. The influences of Ni doping were also investigated through series studies of morphology, structure and electrochromic properties. We found that the optical modulation and coloration efficiency of WO_3 films were significantly enhanced by appropriate amount of Ni doping. Finally, the electrochormic properties of dark ECD assembled with optimized Ni-WO_3 film and NiO-based film were investigated.

2 Experimental

2.1 Materials

All solvents and chemicals were of analytical grade and used without further purification. All the materials were purchased from Sinopharm Chemical Reagent Co. Ltd except for lithium perchlorate ($LiClO_4$, 99% anhydrous), titanium ipropoxide ($Ti(OC_3H_7)_4$) and poly(methyl methacrylate) (PMMA) which were purchased from Sigma Aldrich.

2.2 Preparation of Ni-WO_3 films

Ni-WO_3 nanostructure films were directly prepared on ITO coated glass through hydrothermal oxidation method. Firstly, 1.65 g $Na_2WO_4{\cdot}2H_2O$ and 2.64 g $(NH_4)_2SO_4$ were dissolved in 38 ml de-ionized water. Then 3 M HCl was slowly dropped into the solution under vigorous stirring to adjust the PH value to 2.0. Thereafter, different atomic percentages of Ni source (0, 0.5, 1.5 and 2.5 %) were added into the solution under stirring. The precursor solution was obtained after $NiNO_3{\cdot}6H_2O$ was completely dissolved. Afterwards, the precursor solution was transferred into a Teflon-lined stainless autoclave. The ITO coated glass was placed vertically in the autoclave and the hydrothermal oxidation was carried out at 180 ℃ for 1~3 h to maintain the thickness of the films to be around 600 nm. Finally, the as-deposited films were washed and dried in air at 60 ℃ for 12 h. Furthermore, 1.5% Ni-WO_3 films with areas for about 5×5 cm^2 were prepared to assemble ECD in the same way with twice volume of the solution reacted in 100 ml autoclave.

2.3 Preparation of Li-Ti-NiO films

Li-Ti-NiO films were prepared by sol-gel spin coating method as described in our previous report.[27] In brief, 0.4 M $Ni(CH_3COO)_2{\cdot}4H_2O$ and 0.2 M CH_3COOLi were dissolved in 50 ml ethanol first, then 0.1 M $Ti(OC_3H_7)_4$ was added to the solution under stirring. The sols were stirred for 30 min and filtered with a 0.22 μm Teflon filter. The fresh prepared sols were then spin-coated on the ITO substrates at 2000 rpm for 30 s. After spin coating, the films were sintered at 300 ℃ for 30 min. The spin coating and heating process were repeated twice to obtain films of double layers. The thickness of Li-Ti-NiO film is about 260 nm.

2.4 EC devices assembly

The Ni-WO_3 films were used as working electrode to assemble electrochromic devices with Li-Ti-NiO films. To assemble the electrochromic device, the working and counter electrodes were placed face to face and sealed around leaving one injection port. In this process, UV-curable sealant was used as hermetic gasket to seal the device and 100 μm glass beads as spacer to control the thickness of the device. Then 1 M $LiClO_4$-propylene carbonate ($LiClO_4$-PC) electrolyte solution was injected into the space between the two electrodes. Finally, the injection port was sealed with UV-curable sealant.

The Ni-WO_3 and Li-Ti-NiO films were further applied in all solid ECD by using PMMA based $LiClO_4$ containing solid polymer electrolyte (SPE).[28] SPE was synthesized by dissolving PMMA, PC and $LiClO_4$ in tetrahydrofuran (THF). The mixture was then cast onto a clean glass dish and get dried at room tempreture for about 24 h. The self-standing SPE was obtained by peering it off from the dish. Finally, the all solid ECD was fabricated by sandviching this SPE between the two electrochromic films.

2.5 Characterization

The crystalline structure of the Ni-WO_3 films were examined by X-ray diffraction (XRD) analysis (X'Pert PRO; PANalytical B. V., Almelo, Netherlands) with Cu-K_α radiation in the range of 10-70º of 2θ. The composition of the films were measured by X-ray photoelectron spectroscopy (XPS, ESCALAB 250; Thermo-VG Scientific, East Grinstead, West Sussex, UK) using an Al-K_α as the X-ray source and inductively couple plasma mass spectrometer (ICP-MS; PlasmaQuad3, Thermo-VG, USA). The surface morphology and structure of the films were determined by field emission scanning electron microscopy (FE-SEM; Sirion 200, FEI, Hillsboro, Oregon, USA) and transmission electron microscopy (TEM; JEM-2011, Japan). The thicknesses of the films were measured by using the standard scan of a surface profiler (Dektak 150; Veeco, Tucson, Arizona, USA).

Electrochemical and optical properties of Ni-WO_3 films and ECD were investigated by using electrochemical analyser (CHI-650D; CH Instruments, Shanghai, China) and UV-vis-NIR spectroscopy (V-670; Jasco, Tokyo, Japan). Cyclic voltammetry (CV) and chronocoulommetry (CC) methods were carried out in 0.1 M $LiClO_4$-PC electrolyte in a standard three-electrode cell with platinum (Pt) as counter electrode, silver (Ag) wire as reference electrode and the films as working electrodes at room temperature. Electrochemical impedance spectrum (EIS) tests were conducted on the electrochemical workstation (CHI-660; CH Instruments, Shanghai, China) at open-circuited potential in the frequency range of 0.1 HZ-100 kHZ in 0.1 M $LiClO_4$-PC electrolyte.

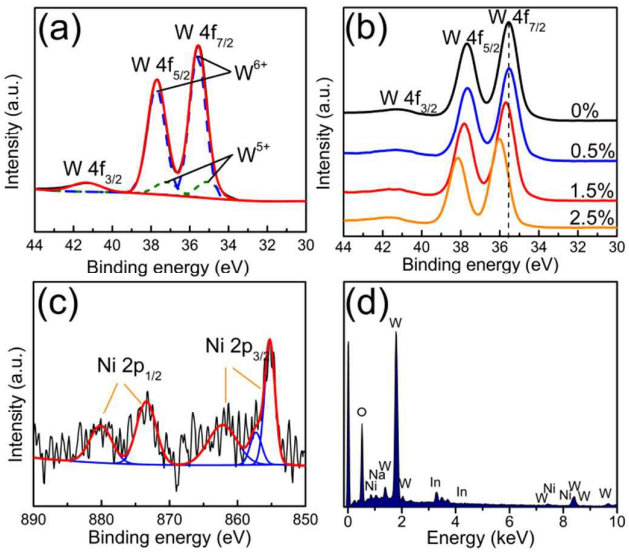

Fig. 1. W 4f XPS spectra of undoped WO_3 film (a), Ni-doped WO_3 films (b) and Ni 2p XPS spectra of 2.5% Ni-doped WO_3 film (c), and EDS mapping analysis of 2.5% Ni-doped WO_3 film (d).

Table 1 Ni concentration in Ni-WO_3 films detected by XPS and ICP-MS, and the mol ratio of W^{6+}/W^{5+} in the four kinds of films calculated from XPS fitting peaks.

Ni-WO_3	Mol(Ni/W) (%)		W^{6+}/W^{5+}
	XPS	ICP-MS	
0%	0	0	6.75
0.5%	2.15	2.53	7.88
1.5%	4.89	4.95	10.3
2.5%	5.86	6.11	19.0

3 Results and discussion

3.1 Structure and morphology of Ni-WO_3 films

XPS was applied to identify elements and analyse their corresponding valence states in the Ni-WO_3 films in our present work. A typical survey spectrum of 2.5% Ni-WO_3 film (Fig. S1 shown in supplementary data available online) verified the co-existance of W and Ni in the film.The detailed W 4f and Ni 2p core-level XPS spectra of Ni-WO_3 films fitted by using XPS peak 4.1 software are presented in Fig. 1. For undoped WO_3 film shown in Fig. 1a, the well-resolved peaks (solid lines) at binding energy of 35.5, 37.7 and 41.3 eV can be assigned to the spin-orbit split peaks of W $4f_{7/2}$, W $4f_{5/2}$ and W $4f_{3/2}$, respectively.[29, 30] The fitting peaks (dot lines) at higher binding energies in the W $4f_{7/2}$ and W $4f_{5/2}$ doublet can be ascribed to W^{6+}, and those at lower binding energies can be attributed to W^{5+}.[17, 18, 29] As shown in Fig. 1b, the W 4f peaks shift to higher binding energy as doping Ni concentration increases, indicating that W^{6+} component increases with Ni doping. To make the variation of W^{6+} content more clearly, the ratio of W^{6+}/W^{5+}, which is approximate to fitting peaks area ratio, is calculated and listed in Table 1 (fitting peaks for four kinds of Ni-WO_3 films presented in Fig. S2 available in supplementary data online). The Ni 2p XPS spectrum of the 2.5% Ni-WO_3 film is shown in Fig. 1c. The peaks at binding energy of 850-870 eV and 870-885 eV can be indexed to Ni $2p_{3/2}$ and Ni $2p_{1/2}$ respectively, which could index the existence of Ni in the film.[31] As the noise ratio of Ni 2p XPS is very low, we reconfirmed the composition of the 2.5% Ni-WO_3 film with EDS mapping analysis as shown in Fig. 1d. The data of EDS ascertain the co-existence of Ni and W ions in the films. The molar ratio of Ni/W in the films detected by XPS and ICP-MS shown in Table 1 are approximate, illustrating that the composition of the films are WO_3, $Ni_{0.025}$-WO_3, $Ni_{0.05}$-WO_3 and $Ni_{0.061}$-WO_3.

XRD was taken to investigate the influence of doping Ni ions to the crystalline structure of WO_3 films. As shown in Fig. 2, the diffraction peaks of undoped WO_3 and low concentration Ni-WO_3 film can be indexed to hexagonal phase of WO_3 (JCPDS 85-2460), and diffraction peaks of monoclinic structure $W_{18}O_{49}$ (JCPDS 71-2450) occurs in 2.5% Ni-WO_3 films. For undoped WO_3 film, six diffraction peaks in the spectra can be assigned to (100), (002), (102), (200), (202) and (004) crystal planes, respectively. The intensity of (002) crystal plane is much higher than other diffraction peaks, which implies that the undoped WO_3 prefers to grow along the c-axis [0001].[19] For Ni-WO_3 films, the positions of (002) and (200) peaks slightly shift to higher degrees as the concentration of Ni increases, indicating that lattice spacing of WO_3 films decreases with Ni doping. Moreover, the intensity of (002) decreases while that of (100) and (200) crystal plane becomes stronger with the increase of doping amount of Ni. These variation of intensity of (002) diffraction peaks relative to (100) and (200) crystal plane disclose the change of lattice orientation of WO_3 crystalline structure by Ni doping. Moreover, two new diffraction peaks emerges at 2θ of 15.0 and 28.6 degree in 2.5% Ni-WO_3 film. These two diffraction peaks could be indexed to the (201) and (310) crystal plane of monoclinic $W_{18}O_{49}$ structure, which indicating that 2.5% Ni-WO_3 contains mixture of hexagonal WO_3 and monoclinic $W_{18}O_{49}$ crystal structure. Therefore, Ni doping influences the crystalline orientation and even the crystal phase of WO_3 films. Furthermore, no obvious peaks related to NiO, $NiWO_4$ or other impurities are detected in the XRD of Ni-WO_3 films, revealing that Ni ions may insert into the WO_3 crystalline structure and induce to the variation of WO_3 crystalline structure. Combining the phenomena shown in XPS (Fig. 1), these results indicate that doped Ni^{3+} (0.60 Å) ions may incorporate into WO_3 lattice, occupy the lattice sites of tungsten ions, distorts the crystal structure and decrease the amount of W^{5+} (0.62 Å), thus changing the lattice orientation and reducing the lattice distance of films.

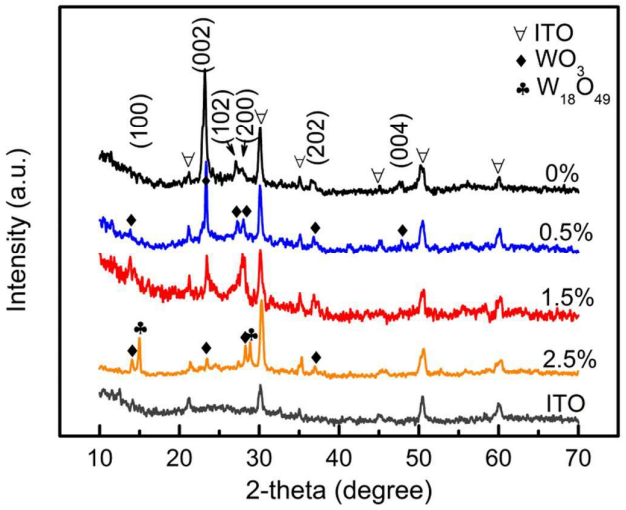

Fig. 2. XRD patterns of Ni-WO_3 films with different Ni content. (hkl) parameters refer to the hexagonal phase of WO_3. Peaks marked by dimond are attributed to hexagonal structure WO_3, while the flower for monoclinic structure $W_{18}O_{49}$.

The surface SEM images of Ni-WO_3 films with different doping Ni concentration is shown in Fig. 3. The surface morphology of WO_3 films varies as Ni content increases. For undoped WO_3 film (Fig. 3a), the SEM image illustrates classical porous interwoven network structure composed of nanowires.[19] When WO_3 is doped with 0.5% Ni, the film is nanorods array structure vertically aligned to the surface (cross section images presented in Fig. S3 of supplementary data available online). As for 1.5% Ni-WO_3 film, nanorods are randomly and densely arrayed with branches existing around the surface of the nanorods. When doping Ni content increases to 2.5%, the film becomes compact with nanorods interconnected with each other and nanoflowers composed of nanopaltes occurs on the surface. To verify the variation tendency of WO_3 films by Ni doping, we studied the surface morphology of films with doping Ni content of 0-3% (Fig. S3 in supplementary data available online). SEM images indicates that Ni doping can lead to significant structural change of WO_3 films. For low concentration Ni-WO_3 films, the surface become denser with increasing amount of branches and more wildly arranged nanorods induced by increasing doping Ni content. As doping Ni content is over 2.5%, nanorods gradually disappear and nanoflowers composed of nanoplates occurs.

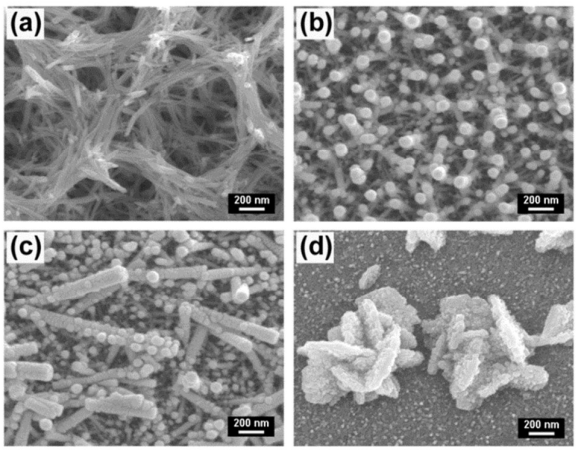

Fig. 3. Surface FE-SEM images of WO_3 films doped with different Ni content; (a) 0%, (b) 0.5%, (c) 1.5% and (d) 2.5%.

It is well known that the anisotropic growth of WO_3 nanostructures can be explained by the specific absorption of ions to particular crystal surface, thus inhibiting the growth of these faces.[32] Therefore, the morphology of WO_3 films can be determined by the crystal growth direction. To further investigate the growth process of Ni-WO_3 nanostructures, powders scraped from these films are investigated by TEM, as displayed in Fig. 4. From the low magnification images, the undoped WO_3 is composed of nanowires with diameter of about 15 nm (Fig. 4a). For 0.5% Ni-WO_3 shown in Fig. 4b, the diameter of naonrod increases to about 25-30 nm and secondary short branches with diameter of about 15 nm grow vertically on the nanorod. For 1.5% Ni-WO_3, the diameter of nanorods is about 40 nm with increasing amount of secondary WO_3 braches vertically and randomly grown around. When the doping amount of Ni ions increases to 2.5%, nanorods aggregates and lamellar structures appears (Detailed TEM images for 2.5% Ni-WO_3 shown in Fig. S4 in supplementary data available online). As the addition of Ni doping ions, the size of the nanosturcture increases and different nanostructures such as branches and lamellar structures form. To determine the growth direction of these nanostructures, we further collected high-magnification images of TEM. As shown in Fig. 4e, the regular spacing of the lattice fringes of undoped WO_3 are found to be about 0.383 nm, corresponding to the (002) plane of hexagonal WO_3 crystal. This result confirms that the nanowires of undoped WO_3 grow along the (002) direction (c-axis). For low concentration Ni-WO_3, the trunks of the nanostructure all grow along (002) and the spacing of (002) plane decreases as the Ni content increases. The spacing of the branches in low concentration Ni-WO_3 (0.5% and 1.5%) is about 0.327nm and 0.315 nm respectively, which could be indexed to (200) planes of hexagonal WO_3. This result illustrates that the growth direction of the branches is vertical to that of the trunk. For 2.5% Ni-WO_3, the lattice spacing of lamellar structure is about 0.588 nm, corresponding to the (201) plane of monoclinic $W_{18}O_{49}$. The microstructure and lattice fringes are consistent with the results of SEM and XRD.

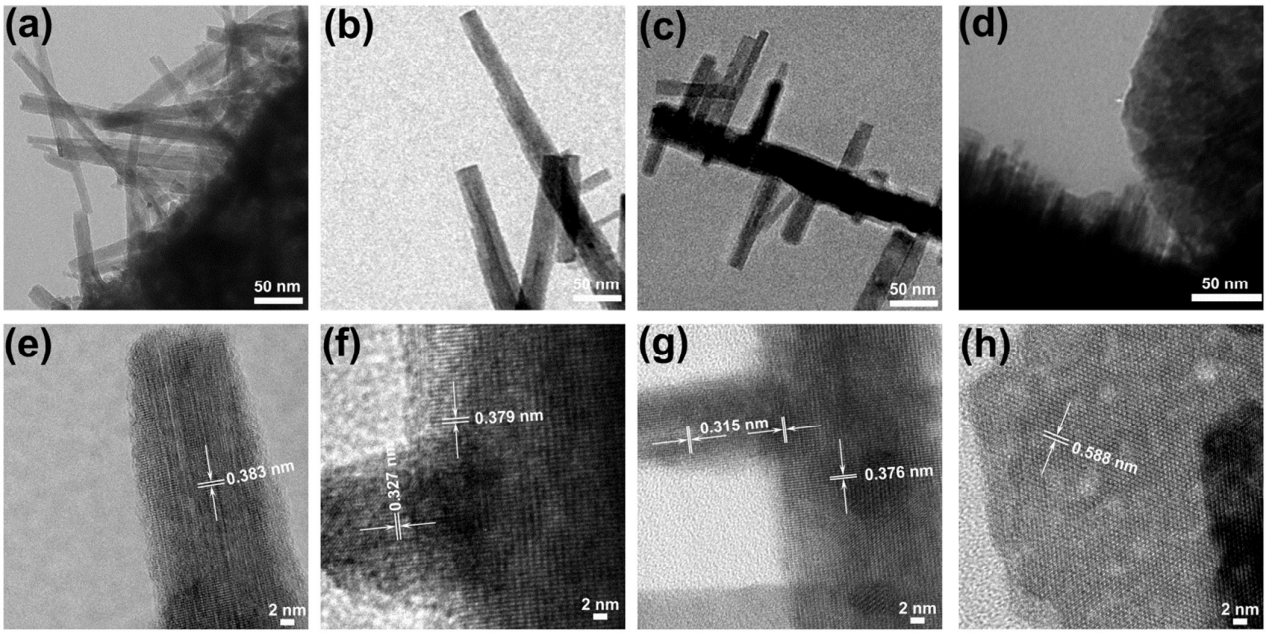

Fig. 4. Low magnification (a-d) and high manification (e-h) TEM images of NiO-WO_3 films with different Ni content : (a) and (e) 0%, (b) and (f) 0.5%, (c) and (g) 1.5%, (d) and (h) 2.5%.

During the hydrothermal synthesis process, WO_3 nanowires were formed by preferentially absorption of sulfate ions on the faces parallel to (002) crystal plane.[32] As low concentration doping Ni ions intercalated into the WO_3 crystalline structure, the crystal structure of WO_3 hexagonal crystal were distorted and lattice defect increased. Doping Ni ions inhibits the growth of (002) crystal plane, while (200) plane, which is perpendicular to (002) plane, grew from the defects and around the trunk of nanowire, thus forming vertically grown branches. As doping Ni content continued to increase, part of WO_3 turned into monoclinic $W_{18}O_{49}$ crystal structure and formed nanoplate structure.

3.2 Electrochromic properties of Ni-WO_3 films

In order to identify ions insertion/extraction process during the electrochromic reaction of Ni-WO_3 films, CV measurements were conducted in 0.1 M $LiClO_4$/PC electrolyte with the potential range of -1.5 V to 1 V at a scan rate of 50 mV/s. Fig. 5 compares the second CV curves of Ni-WO_3 films with different Ni concentration. During the cycling, visible color change takes place accompanied by the intercalation/deintercalation of Li^+ ions into/out of WO_3 films. The electrochromic process of WO_3 films could be described as the following formula (1):

$$WO_3(bleached) + \mathrm{x}Li^+ + xe^- \leftrightarrow Li_xWO_3(colored) \qquad (1)$$

From CV curves shown in Fig. 5, we find that both the anodic and cathodic current density are larger than those of undoped WO_3 film, and increase with Ni doping amount and then decreases when the concentration of Ni reaches 2.5%. This similar trend also goes with the position of anodic peak as it increases with Ni doping amount while decreases for 2.5% Ni-WO_3. The increasing of current density and shift of peak position for 0.5% and 1.5% Ni-WO_3 films demonstrate that low-concentration Ni doping accelerates the electrochromic reaction activity in the films. These enhancement can be attributed to the vertically arrayed microstructure of 0.5% and 1.5% Ni-WO_3 films, which could provide more effective contacting surface area with electrolyte. For 2.5% Ni-WO_3 film, the surface become denser, which may impede the charge transfer of ions and lower the peak current density.

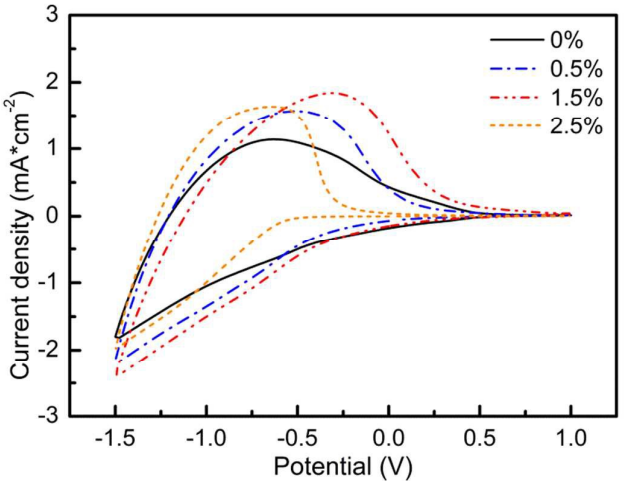

Fig. 5. The 2nd cyclic voltammetry (CV) curves of Ni-WO_3 films with different Ni content in potential range of -1.5-1 V at a scan rate of 50 mV/s in 0.1 M $LiClO_4$/PC electrolyte using Ag wire as the reference electrode.

The optical modulation properties of Ni-WO_3 in visible and near-infrared region were measured after CV tests for three cycles. Fig. 6 displays the transmittance spectra of Ni-WO_3 films in bleached (solid line) and colored (dotted line) states at wavelength from 380 nm to 1000 nm. For 0-1.5% Ni-WO_3 films, the transmittance modulation in both visible and near-infrared region increases with Ni doping, from 50.9% to 86.0% at 600 nm and from 62.2% to 85.9% at 900 nm. Moreover, 1.5% Ni-WO_3 film exhibits excellent transmittance modulation of over 85% at the wavelength from 600 nm to 1000 nm. When Ni doping concentration reaches 2.5%, the transmittance modulation decreases sharply, and the transmittance of bleached state is lower than that of colored state in the visible region. The haze of the 2.5% Ni-WO_3 film measured at bleached and colored state is 76.3% and 59.5% respectively, which could be the reason of abnormal variation of transmittance measured in the visible region. As shown in Table 2, the haze of Ni-WO_3 films increases with Ni doping content which could be attributed to the gradual denser nanostructure morphology of the films. These results discloses that even little amount of Ni ions doping can influence the electrochromic properties of WO_3 films and there is an optimized content of doping Ni ions.

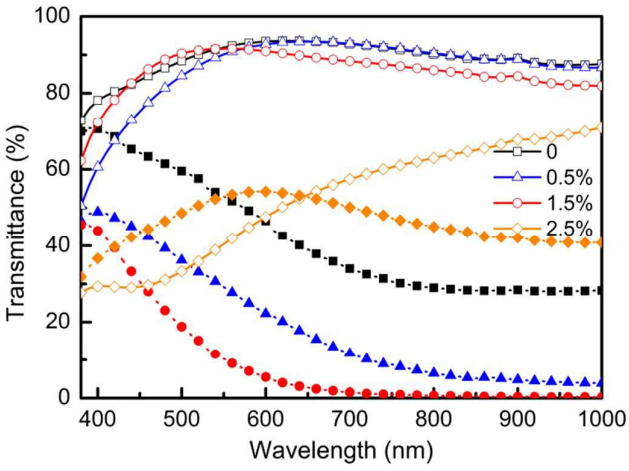

Fig. 6. Transmittance spectra of Ni-WO_3 films at bleached (solid line) and colored (dotted line) state tested right after 3 CV cycles, applied at +1 V, 60 s and -1.5 V, 60 s respectively in 0.1 M $LiClO_4$-PC electrolyte with three-electrode system.

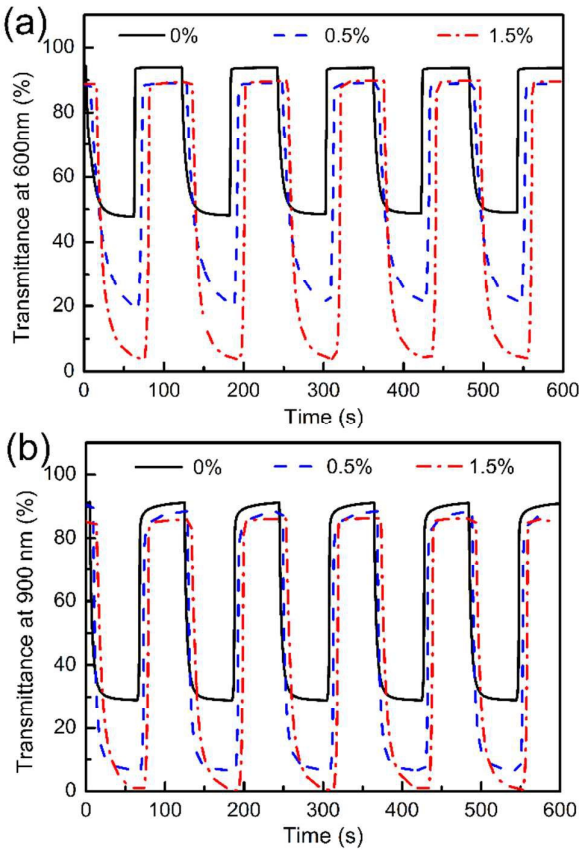

Fig. 7. Optical transmittance response at 600 nm (a) and 900 nm (b) of Ni-WO_3 films applied at +1 V and -1.5 V for 60 s in $LiClO_4$-PC electrolyte with three-eletrode system.

The response time is also an important parameter for electrochromic films. As the optical modulation properties of 2.5% Ni-WO_3 is very low, we just compared the response time of 0-1.5% Ni-WO_3 films. Fig. 7 shows transmittance data measured at 600 nm and 900 nm by switching the potential between -1.5 V and +1 V for 60 s. The response time is defined as the time it takes to reach 90% of the maximum transmittance modulation at a defined wavelength, and the values of response time, charge density and other electrochromic properties of the films are also listed in Table 2. For Ni-WO_3 films, the response time for bleaching process slightly extends as Ni concentration increases, which could be attributed to the increased charge density inducing to larger amount of Li ions that should be extracted from the film during the bleaching process. In the coloring process, 0.5 % Ni-WO_3 film is a little faster than the undoped WO_3 film, while 1.5% Ni-WO_3 film needs much longer time to get fully colored. The result indicates that vertically alined nanorods morphology and defected crystalline sturcture could facilate the insertion/ extraction process of Li^+ ions. The decreased switching speed of 1.5% Ni-WO_3 film could be due to the serried arrangement of the branched nanorods, which is difficult for the insertion of Li^+ ions into the film.

Table 2 Various electrochromic properties of Ni-WO_3 films with different Ni concentration.

Ni-WO_3	Haze (%)	ΔT [a] (%)		Charge density (mC cm^{-2})	Response time [b] (s)		R_{ct} [c] (Ω cm^2)	Conductivity [d] (S cm^{-1})
		600 nm	900 nm		t_b	t_c		
0%	7.3	50.9	62.2	18.2	4.8	8.6	14.57	4.12E-6
0.5%	28.9	67.8	82.0	19.4	6.0	7.8	9.22	6.51E-6
1.5%	36.3	86.0	85.9	24.6	6.2	19.0	64.54	9.30E-7
2.5%	76.3	-9.2	25.7	17.8	-	-		

[a] ΔT: the variation between transmittance of bleached and colored state.

[b] Response time: the time the materials takes to reach 90% of the maximum transmittance modulation at a defined wavelength.

[c] R_{ct}: charge-transfer resistance calculated from EIS data using Zview software.

[d] Conductivity: electric conductivity through the film calculated from R_{ct} .

To further understand the charge transfer process during the coloring process in Ni-WO_3 films, EIS were conducted at their open-circuited potential (about -0.3 V) in 0.1 M $LiClO_4$-PC electrolyte. The EIS results shown in Fig. 8 consists of a semicircle in high frequency region and a straight line in low frequency region, which is related to charge transfer resistance and ions diffusion resistance, respectively.[20, 23] The enlarge view of high frequency part is displayed in the inset at the right top corner of Fig. 8. The size of semicircle in high frequency part of EIS relates to charge transfer resistance (R_{ct}) of Ni-WO_3 films, and it is well accepted that smaller semicircle means a lower charge transfer resistance. The comparison of EIS plots of Ni-WO_3 films indicates that 0.5% Ni-WO_3 film exihibites smaller R_{ct} than the other two. As presented in Table 2, R_{ct}, calculated by simulating EIS plots using equivalent circuit (shown in Fig. S5 and Table S1 in supplementary data available online), decreases with 0.5% Ni ions doping and increases with 1.5% Ni doping. The variation of correspoding conductivity of Ni-WO_3 films, calculated from R_{ct} (formula (1) shown in supplementary data available online), indicates that the vertically aligned nanorods provide more free space for Li^+ ions insertion and make the ions transfer easier. For 1.5% Ni-WO_3 film, the intensively arrayed nanorods inhibits the insertion process of Li^+ ions into the films.

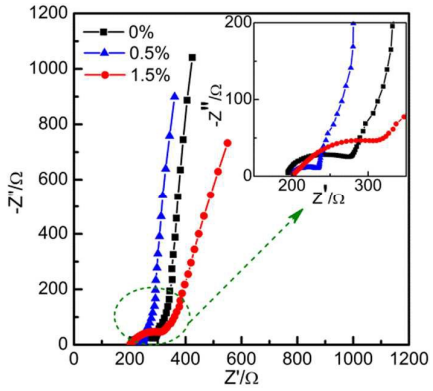

Fig. 8. EIS data for Ni-WO_3 films measured at open-circuited potential with inset graph of expansion in high frequency region. Measured data were taken at -0.3 V vs. Ag reference in 0.1 M $LiClO_4$-PC electrolyte.

Coloration efficiency (CE) should also be taken into consideration to assess the optimized Ni-WO_3 films. CE is defined as the changes in optical density (ΔOD) per unit of electrode area at a given wavelength, which can be calculated from the following equation (2):[33]

$$\mathrm{CE} = \Delta OD/Q = \log(T_b/T_c)\,/Q \qquad (2)$$

Where Q is the integration of current within the colored time per unit of electrode area, and T_b and T_c denotes the transmittances of the bleached and colored states, respectively. Fig. 9 presents the curves of ΔOD at wavelength of 600 nm versus the inserted charge density at a potential of -1.5 V. CE of Ni-WO_3 films could be calculated from the slop of these curves. The CE is 37.1 and 60.5 $cm^2\,C^{-1}$ for 0.5% and 1.5% Ni-WO_3 film, respectively, which is larger than that of undoped WO_3 film (20.8 $cm^2\,C^{-1}$). Furthermore, CE of Ni-WO_3 films over the entire transmittance luminous spectrum at 380-1000 nm (Fig. S6 in supplementary data available online) increases in near-infrared region, and even reaches about 120 $cm^2\,C^{-1}$ for 1.5% Ni-WO_3 films. These results demonstrate that Ni-WO_3 films have good optical modulation in near-infrared region, and low concentration Ni doping can enhance CE of WO_3 films.

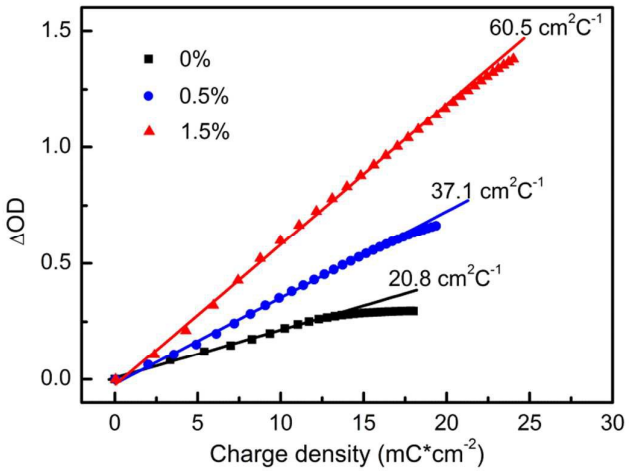

Fig. 9. Variation of the optical density (ΔOD) vs. charge density for Ni-WO_3 films at 600 nm measured at -1.5 V for 60 s in 0.1 M $LiClO_4$-PC electrolyte versus Ag reference.

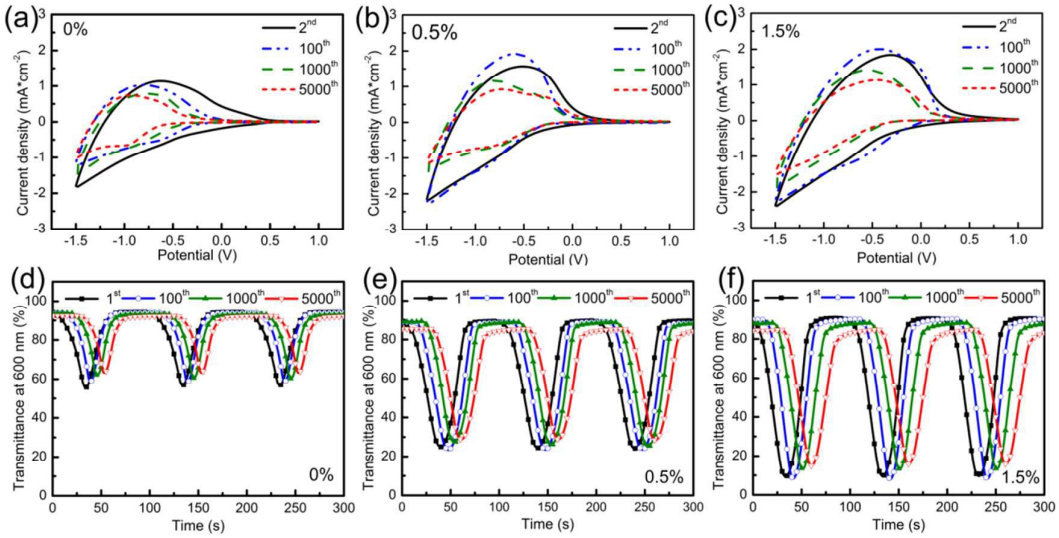

Fig. 10. CV cycling stability (a-c) and the corresponding transmittance (d-f) of Ni-WO_3 films with different Ni doping concentration. CV data for different cycle numbers in potential range of -1.5-1 V at scan rate of 50 mV/s in 0.1 M $LiClO_4$-PC electrolyte for (a) 0%, (b) 0.5% and (c) 1.5% Ni-WO_3 films. Optical transmittance response at 600nm corresponding to different CV cycles shown in (a-c) for (d) 0%, (e) 0.5% and (f) 1.5% Ni-WO_3 films.

The cycling stability of Ni-WO_3 films were also an important parameter for the future applications of electrochromic materials. We performed continuous CV cycling and corresponding in-situ transmittance tests at 600 nm for 0-1.5% Ni-WO_3 film at -1.5-1V with scan rate of 50 mV s^{-1}. As shown in Fig 10 (a) and (d), pure WO_3 films undergoes continuous degration in both current density and optical modulation, which could be assigned to ion-trapping-induced degradation during the cycling.[34] As for 0.5% and 1.5% Ni-WO_3 films, the current density and optical modulation increase in the fist 100 cycles, which could be attributed to the activation process of the film.[35] During this activation process, the thickness that Li^+ ions insterted into the films increases and the amount of WO_3 that participated in the electrochromic redox process increases, thus inducing to the enhanced current density and optical modulation. After the activation process, the electrochrmic performance of 0.5% and 1.5% Ni-WO_3 shows similar degration trend to the pure WO_3 film. To see the degration trend clearly, the corresponding in-stiu transmittance of Ni-WO_3 films in bleached and colored state at 600 nm are presented in Fig. 11. During the 5500 CV cycling test, three kinds of Ni-WO_3 films exhibites good cycling stability with about 10% contrast loss. 0.5% and 1.5% Ni-WO_3 films sustain a transmittance modulation of about 85.9% (from 65.2% to 56.0%) and 86.8% (from 80.2% to 69.6%) of their initial value after 5500 cycles, while pure WO_3 for about 73.8% (from 38.6% to 28.5%). These results indicate that the vertically alined nanorods morphology and defected crystalline structrue of 0.5% and 1.5% Ni-WO_3 films facilate the ectraction process of Li^+ ions and decrease the traping ions during the cycling, thus increasing the cycling stability of WO_3 films.

Therefore, electrochemical and optical properties depend on the concentration of Ni doping in WO_3 films. Electrochromic properties of WO_3 films could be enhanced with low amount of Ni doping and decreased with high concentration (2.5%). 1.5% Ni-WO_3 film, as the optimized one, exhibites excellent optical modulation for about 85%, high CE of about 120 cm^2 C^{-1} and good cycling stability for about 5500 cycles. These electrochromic properties are comparable with Ti-doped WO_3, vertically aligned WO_3 nanostructure films, WO_3 nanoparticle and quantum dots films as reported before.[17, 18, 20, 23] The response speed in our work is enhanced as compared to bulk WO_3 films, but is still very slow as compared to 1.0 s of WO_3 quatum dots.[16, 18] We have proceed this research and enhancing response speed is also an important study in our future work.

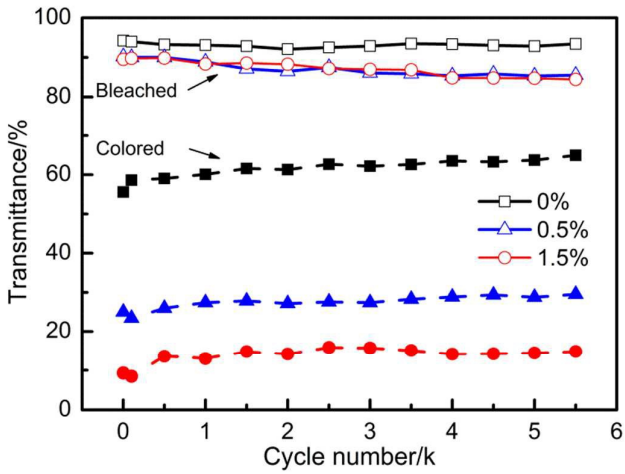

Fig. 11. Optical transmittance stability of Ni-WO_3 films with different Ni concentration at 600 nm wavelength during CV cycles in potential range of -1.5-1 V at 50 mV/s in 0.1 M $LiClO_4$-PC electrolyte

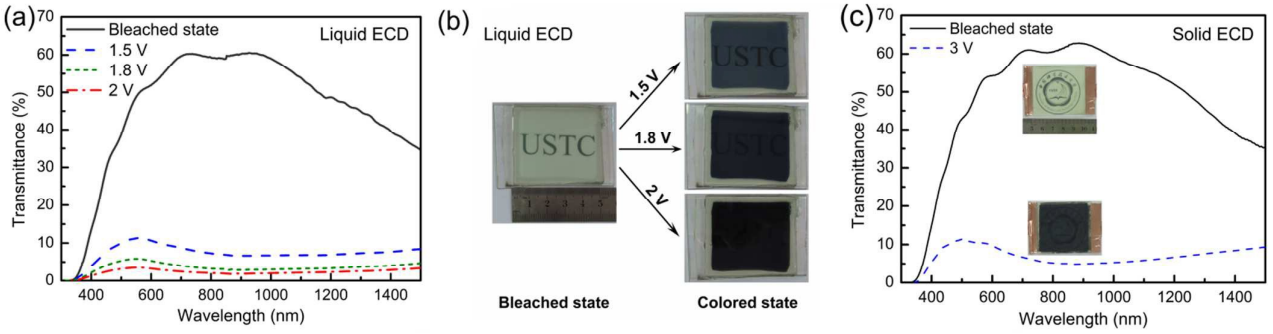

Fig. 12. (a) Optical transmittance spectra of the complementary ECD assembled by 1.5% Ni-WO_3 and Li-Ti-NiO films in bleached (solid line) and colored (dotted lines) state drived at different voltage from 1.5 V to 2 V for 300 s. (b) Corresponding photographs of ECD (5 cm × 5 cm) at bleached state (left) and colored state (right), applied at different potential for 300 s. (c) Optical transmittance spectra and corresponding pictures of all-solid ECD in bleached (solid line) and colored state (dotted line) drived at ±3 V for 30s.

3.3 Performance of ECD

To further investigate the applications of Ni-WO_3 film in ECD, we selected the optimized 1.5% Ni-WO_3 film to assemble a 5cm × 5cm ECD using Li-Ti-NiO film as a counter electrode. Li-Ti-NiO film, shows good optical modulation in the visible region (transmittance spectra of Li-Ti-NiO in Fig. S7 available online), while Ni-WO_3 demonstrates excellent optical modulation in near-infrared region (Fig. 6). Thus, the combination of Li-Ti-NiO film and Ni-WO_3 films in an ECD may exhibit a neutral visual appearance with good optical modulation in both visible and near-infrared region. Fig. 10 demonstrates the optical transmittance spectra and the corresponding photographs of the ECD stimulated at different potential. The transmittance of the ECD in the bleached state (solid line) is found to be about 60% in the near-infrared region of 700-1000 nm. The transmittance of ECD in the colored state (dotted line) decreases as the applied potential increases, and the color of the device darkens from deep blue to almost black while the transmittance accordingly decreases from about 11.4% (maximum) to 3.5% (maximum). The maximum transmittance modulation (ΔT) increases from 53.6% to 58.6% by the increasing of the stimulated potential. Moreover, the CIE 1931 (x, y, Y_L%) numerical data of ECD varies from (x= 0.359, y=0.381, Y_L%= 44.94) in bleached state to (x= 0.326, y= 0.369, Y_L% = 3.29%) in the dark state (under 2 V). Y_L%, which is presented as relative or percentage luminosity, is very low and the position of the dark state in the CIE color space (Fig. S8 in supplementary data available online) is close to the white light, indicating that the color of the device is almost black.

The 1.5% Ni-WO_3 and Li-Ti-NiO films were further applied in an all-solid ECD by using PMMA-$LiClO_4$ based SPE. Fig. 12(c) exhibits the picture of all-solid ECD at its bleached and colored states, and corresponding transmittance spectra. The ECD demonstrates uniform color change from transparent to dark blue with low applied voltage of 3 V (Video of both liquid and solid ECD attached to supplementary data available online). Similar with liquid ECD, all-solid ECD presents good optical transmittance modulation from visible to near-infrared region with maximum transmittance variation of 57.9%. This device demonstrates good optical modulation properties and tuneable colors, which shows promising applications in smart windows.

4 Conclusions

In summary, vertically aligned Ni-WO_3 films were successfully synthesized through seed-free hydrothermal method directly on ITO glass. The morphology, crystal structure and electrochromic properties of Ni-WO_3 films are dependent on the doping Ni concentration. The doping Ni ions intercalate into hexagonal WO_3 crystal structure, increases the ratio of W^{6+}/W^{5+}, and decrease the growth rate of (002) plane, thus changing the nanostructure of the films. The low concentration Ni-WO_3 films illustrates enhanced optical modulation (86% at 600 nm over that of amorphous WO_3 film), coloration efficiency and cycling stability for about 5500 cycles, which could be attributed to the distorted crystalline structure and vertically aligned nanorod structure. When Ni doping concentration increased to 2.5%, monoclinic $W_{18}O_{49}$ crystal structure emerged and the surface of the film became compact, leading to high haze and low transmission modulation. The 1.5% Ni-WO_3 film, as the optimized one, were selected to assemble complementary electrochromic device with Li-Ti-NiO film. When the applied potential increases, the transparent device can be darkened to black, with maximum transmission of about 3.5%. The dark device can find promising applications in architecture and automobile energy-saving smart windows.

Acknowledgements

This work was supported by the National Natural Science Foundation of China (21474096, 21274138, 21273207, 51503193).

References

1 Y. Dong and C. Xu, *International Journal of Nonlinear Sciences and Numerical Simulation*, 2010, **11**, 63-70.

2 K. Tajima, Y. Yamada, S. Bao, M. Okada and K. Yoshimura, *Solar Energy Materials & Solar Cells*, 2008, **92**, 120-125.
3 N. Kobayashi, S. Miura, M. Nishimura and H. Urano, *Solar Energy Materials & Solar Cells*, 2008, **92**, 136-139.
4 G. A. Niklasson and C. G. Granqvist, *J Mater Chem*, 2007, **17**, 127-156.
5 C. Xu, L. Liu, S. E. Legenski, D. Ning and M. Taya, *J Mater Res*, 2004, **19**, 2072-2080.
6 J. H. Zhang, J. P. Tu, D. Zhou, H. Tang, L. Li, X. l. Wang and C. D. Gu, *J Mater Chem C*, 2014, **2**, 10409-10417.
7 B. Moshofsky and T. Mokari, *J Mater Chem C*, 2014, **2**, 3556-3561.
8 F. M. Kelly, L. Meunier, C. Cochrane and V. Koncar, *Displays*, 2013, **34**, 1-7.
9 Y. S. Nam, H. Park, A. P. Magyar, D. S. Yun, T. S. Pollom and A. M. Belcher, *Nanoscale*, 2012, **4**, 3405-3409.
10 H. Moulki, D. H. Park, B. K. Min, H. Kwon, S. J. Hwang, J. H. Choy, T. Toupance, G. Campet and A. Rougier, *Electrochim Acta*, 2012, **74**, 46-52.
11 S. Green, J. Backholm, P. Georen, C. G. Granqvist and G. A. Niklasson, *Solar Energy Materials & Solar Cells*, 2009, **93**, 2050-2055.
12 C. Xu, H. Tamagawa, M. B. Uchida and M. Taya, *Smart Structures and Materials 2002: Electroactive Polymer Actuators and Devices*, ed. Y. BarCohen, 2002, **4695**, 442-450.
13 Z. Hussain, *J Mater Res*, 2001, **16**, 2695-2708.
14 D. M. Welsh, A. Kumar, E. W. Meijer and J. R. Reynolds, *Adv Mater*, 1999, **11**, 1379-1382.
15 J. H. Zhang, G. F. Cai, D. Zhou, H. Tang, X. I. Wang, C.D. Gu and J.P. Tu, *J Mater Chem C*, 2014, **2**, 7013-7021.
16 M. Deepa, M. Kar and S. A. Agnihotry, *Thin Solid Films*, 2004, **468**, 32-42.
17 P. Yang, P. Sun, Z. Chai, L. Huang, X. Cai, S. Tan, J. Song and W. Mai, *Angew Chem In Edit*, 2014, **53**, 11935-11939.
18 S. Cong, Y. Y. Tian, Q. W. Li, Z. G. Zhao and F. X. Geng, *Adv Mater*, 2014, **26**, 4260-4267.
19 J. Zhang, J. P. Tu, X. H. Xia, X. l. Wang and C. D. Gu, *J Mater Chem*, 2011, **21**, 5492-5498.
20 G. F. Cai, J. P. Tu, D. Zhou, X. L. Wang and C. D. Gu, *Solar Energy Materials & Solar Cells*, 2014, **124**, 103-110.
21 J. M. Wang, E. Khoo, P. S. Lee and J. Ma, *J Phys Chem C*, 2009, **113**, 9655-9658.
22 J. M. Wang, E. Khoo, P. S. Lee and J. Ma, *J Phys Chem C*, 2008, **112**, 14306-14312.
23 G. F. Cai, X. L. Wang, D. Zhou, J. H. Zhang, Q. Q. Xiong, C. D. Gu and J. P. Tu, *Rsc Adv*, 2013, **3**, 6896-6905.
24 S. V. Green, E. Pehlivan, C. G. Granqvist and G. A. Niklasson, *Solar Energy Materials & Solar Cells*, 2012, **99**, 339-344.
25 S. V. Green, A. Kuzmin, J. Purans, C. G. Granqvist and G. A. Niklasson, *Thin Solid Films*, 2011, **519**, 2062-2066.
26 Y. R. Hu, L. G. Wang and G. Q. Li, *Plasma Sci Technol*, 2007, **9**, 452-455.
27 J. Zhou, G. Luo, Y.X. Wei, J.M. Zheng, C. Xu, *Electrochim Acta*, 2015, **186**, 182-191.
28 G. P. T. Ganesh, R. Ravi and B. Deb, *Solar Energy Materials & Solar Cells*, 2015, **140**, 17-24.
29 M. Deepa, A. K. Srivastava, S. N. Sharma, Govind and S. M. Shivaprasad, *Appl Surf Sci*, 2008, **254**, 2342-2352.
30 F. Bussolotti, L. Lozzi, M. Passacantando, S. La Rosa, S. Santucci and L. Ottaviano, *Surf Sci*, 2003, **538**, 113-123.
31 S. Oswald and W. Bruckner, *Surf Interface Anal*, 2004, **36**, 17-22.
32 Z. Gu, H. Li, T. Zhai, W. Yang, Y. Xia, Y. Ma and J. Yao, *J Solid State Chem*, 2007, **180**, 98-105.
33 C. G. Granqvist, S. Green, G. A. Niklasson, N. R. Mlyuka, S. von Kraemer and P. Georen, *Thin Solid Films*, 2010, **518**, 3046-3053.
34 R. T. Wen, C. G. Granqvist and G. A. Niklasson, *Nat Mater*, 2015, **14**, 996-1001.
35 A. Al-Kahlout, S. Heusing and M. A. Aegerter, *J Sol-Gel Sci Techn*, 2006, **39**, 195-206.
36

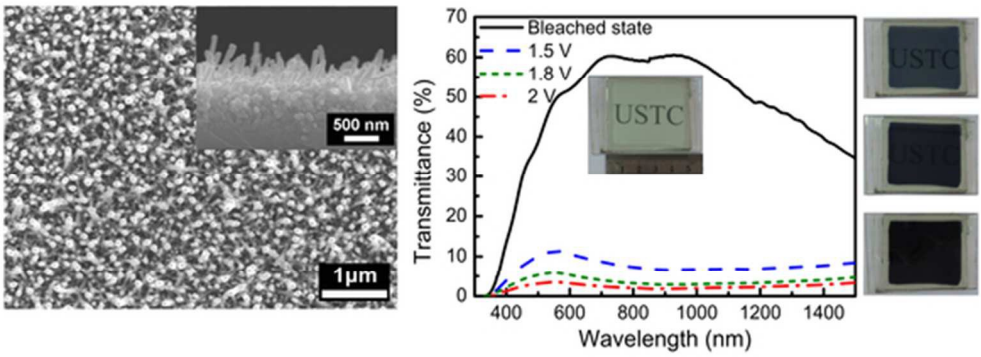

50x19mm (300 x 300 DPI)